1st Virtual European Conference on Fracture

Investigation of the effect of shape of inclusions on homogenized properties by using peridynamics

Yakubu Kasimu Galadima[a,*], Erkan Oterkus[a], Selda Oterkus[a]

[a]PeriDynamics Research Centre, Department of Naval Architecture, Ocean and Marine Engineering, University of Strathclyde, 100 Montrose Street, Glasgow G4 0LZ, UK

Abstract

Fiber-reinforced composite materials are widely used in many different industries due to their superior properties with respect to traditional metals including their light weight, corrosion resistance, high strength, impact resistance, etc. Fiber-reinforced composite materials are composed of a strong fiber material, which mainly carries the applied load, and soft matrix material, which transfers the load to the fiber material and keep the fibers together. Macroscopic analysis of fiber-reinforced composite materials is done by utilising the homogenised material properties which mainly depends on individual material properties of fiber and matrix. In this study, in addition to the effect of individual material properties of constituents, the effect of the shape of fibers (inclusions) on homogenised properties is investigated by using a new methodology called peridynamics.

Keywords: Peridynamics; Homogenisation; Inclusion; Non-local

1. Introduction

Peridynamic (PD) theory was proposed by (Silling, 2000) and essentially replaces the spatial derivatives of the

* Corresponding author. Tel.: +44-141-548-3876.
  E-mail address: yakubu.galadima@strath.ac.uk

classical continuum theory with integral operator which makes the Peridynamic theory capable of admitting discontinuity in the response field. As a result, Peridynamic theory has been successfully applied directly to fracture problems (Basoglu et. al., 2019; De Meo et. al., 2016, 2017; Imachi et. al., 2019, 2020; Kefal et. al., 2019; Liu et. al., 2018; Madenci and Oterkus, 2014; Oterkus et. al., 2010a,b, 2012, 2014; Oterkus and Madenci, 2012a,b; Vazic et. al., 2017, 2020; Wang et. al., 2018; Yang et.al., 2019; Zhu et. al., 2016).

   The increasing requirement for cost efficiency in engineering systems is adding complexity to design requirement. This requirement is making weight saving a critical selection driver in the design of systems in offshore, civil, automobile, and aerospace industries. In response, composites are nowadays used extensively in a wide spectrum of applications. This is because composites offer several attractive attributes that make them better alternative to traditional materials such as steel and aluminium. This has resulted in a growing interest to apply Peridynamics in studying the behaviour of composites (Oterkus and Madenci, 2012; Hu et. al., 2011, 2014, 2015; Guo et. al., 2019; Jiang et. al., 2019; Askari et. al., 2006; Radel et. al., 2019; Baber et. al., 2018; Diyaroglu et. al., 2016; Oterkus, 2010; Ren et. al., 2018; Rokkam et. al., 2018). This growing interest has also motivated the development of homogenization schemes for composites in the framework of Peridynamics. The first attempt at extending the classical locally elastic computational homogenization to the Peridynamic framework was undertaken by (Madenci et. al., 2017) in which the Peridynamic unit cell was developed and a microstructure informed effective properties of composites were computed. A volumetric Periodic Boundary Condition for computational homogenization of peristatic periodic structured composites was proposed in (Buryachenko, 2019). Utilizing a new bond based PD model developed in (Madenci et. al., 2019), a scheme for homogenization of microstructures with orthotropic constituents in finite element framework was proposed in (Diyaroglu et. al., 2019). A method for Representative Volume Element homogenization based on the bond based PD theory was also proposed in (Xia et. al., 2019).

   The focus in this work is to study the effect of inclusion shape on the effective properties of composite materials. To achieve this goal, a homogenization scheme is developed and validated and a method of recovering stress field by postprocessing the results obtained from PD simulation is proposed.

2. Bond-based peridynamics

   In the 'bond-based' Peridynamics, if B is a peridynamic body, then the motion of every point $\mathbf{x} \in B$ is governed by the equilibrium equation:

$$\rho(\mathbf{x})\ddot{\mathbf{u}}(\mathbf{x},t) = \int_{H_x} \mathbf{f}\big(\mathbf{u}(\mathbf{x}',t) - \mathbf{u}(\mathbf{x},t), \mathbf{x}' - \mathbf{x}\big) dV_{\mathbf{x}'} + \mathbf{b}(\mathbf{x},t) \tag{1}$$

where $\ddot{\mathbf{u}}$ is the acceleration vector field, $\mathbf{u}$ is the displacement vector field, $H_{\mathbf{x}}$ is the neighbourhood of the particle located at point $\mathbf{x}$ and $\mathbf{f}$ is a vector valued pairwise force function and represents the force per unit volume squared that particle $\mathbf{x}'$ exerts on particle $\mathbf{x}$. If linear elastic behaviour is assumed, then Eq. (1) specialises to

$$\rho(\mathbf{x})\ddot{\mathbf{u}}(\mathbf{x},t) = \int_{H_{\mathbf{x}}} C(\mathbf{x},\mathbf{x}')\big(\mathbf{u}(\mathbf{x}',t) - \mathbf{u}(\mathbf{x},t)\big) dV_{\mathbf{x}'} + \mathbf{b}(\mathbf{x},t) \tag{2}$$

where $C: B \times B \to \ell$ is a tensor valued micromodulus function that contains intrinsic material properties of B. The PD equilibrium equation Eq. (1) or its linearized version Eq. (2) give rise to integro-differential equations that are defined within the material horizon. Different numerical techniques have been developed to approximate the solution of Eq. (1) or Eq. (2) such as the finite element discretization methods (Chen and Gunzberger, 2011; Wang and Tian, 2012), the collocation methods (Evangelatos and Spanos, 2011; Wang and Tian, 2014) and meshfree methods (Seleson and Littlewood, 2016; Silling and Askari, 2005). The numerical approximation adopted in this work is meshfree method proposed in (Silling and Askari, 2005). In this numerical approximation scheme, the region is discretized into nodes. Each node i is assigned a volume V_i and a material model so that the discrete form of Eq. (2) is given by

$$\rho\ddot{\mathbf{u}}_i = \sum_{j}^{N_i} C(\mathbf{x}_j - \mathbf{x}_i)(\mathbf{u}_j - \mathbf{u}_i)V_j + \mathbf{b}_i \tag{3}$$

where N_i is the number of particles within the horizon of the particle located at $\mathbf{x}_i$.

3. Stress computation

Although attempts have been made in developing the concept of stress in the bond based Peridynamic theory (Silling, 2000; Lehoucq and Silling, 2008; Fallah et. al., 2020; Weckner and Abeyaratne, 2005), the notion has generally played less fundamental role in the development and application of the theory. However, since the notion of stress plays a fundamental role in developing computational homogenization, an attempt will be made in this work to develop a procedure to recover stress values at nodal locations. In this scheme, a finite element mesh is superimposed on the discretized PD model as shown in Fig. 1.
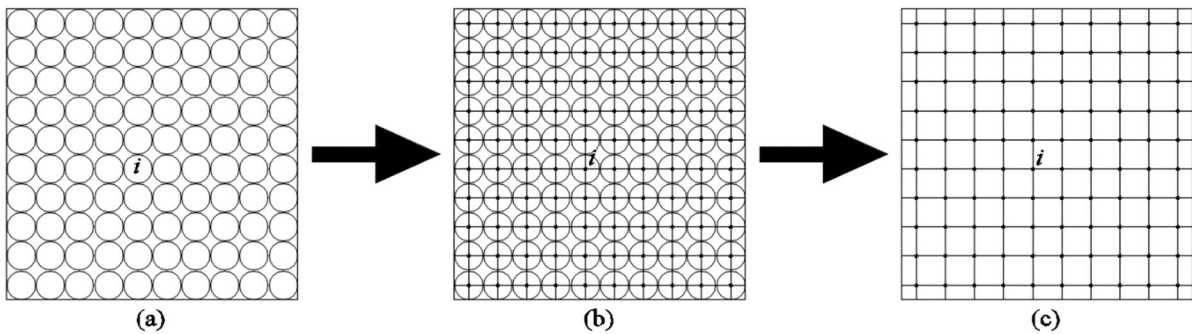

Fig. 1. (a) PD discretization, (b) Superimposition of finite element mesh on PD nodes, (c) Finite element mesh

Once the nodal displacement is obtained from Eq. (3), the procedure of extracting stresses from the displacement result is basically a postprocessing operation and proceeds in the same way as in finite element method. Assuming a linear elastic material, the components of the stress field are given by:

$$\sigma_{ij} = D_{ijkl}\varepsilon_{kl} \tag{4}$$

where D_{ijkl} are the components of the fourth-order stiffness tensor and ε_{kl} are the components of the strain. The strain field in an element is related to the displacement field by

$$\{\varepsilon\} = [B]\{u\}^e \tag{5}$$

where $[B]$ is the strain displacement matrix containing the derivatives of the shape functions and $\{u\}^e$ is the nodal displacement of an element. Substituting Eq. (4) into Eq. (5) yields:

$$\{\sigma\} = [D][B]\{u\}^e \tag{6}$$

4. Homogenisation

The objective of this homogenization scheme just like most homogenization schemes is to replace a heterogeneous medium with an equivalent homogeneous continuum. The equivalent homogeneous medium is expected to have the same averaged mechanical properties as the heterogeneous medium. To achieve this transformation, the problem is divided into two scales. The first scale is the microscopic scale. Here, the region occupied by the original heterogeneous medium is divided into Representative Volume Elements (RVEs) (Hill, 1963). The second scale is the macroscale in which the original heterogeneous medium is replaced with an equivalent homogeneous medium.

Let the region occupied by a RVE in the microscale be Ω, and let $\partial\Omega$ and V be the boundary surface and volume of the RVE, respectively. Let this RVE be assigned to a point in the region occupied by the whole medium. Let $\bar{\Omega}$ be the region occupied by a homogeneous representation of the original medium and let $\partial\bar{\Omega}$ and $\bar{V}$ be the boundary surface and volume of this region. Hereinafter, quantities associated with the macroscale will be denoted with an overbar. The goal in this homogenization scheme is to connect the macroscopic quantities ($\bar{\sigma}$ and $\bar{\varepsilon}$) through the volume averaging of their microscopic counterparts (σ and ε). This is achieved using the standard averaging tools of micromechanics, the Hill-Mandel theorem and application of appropriate boundary conditions.

4.1. Representative Volume Element (RVE)

Central to any discussion on computational homogenization is the concept of the Representative Volume Element (RVE). The notion of RVE adopted in this work is the working definition given in (Yu, 2016) as any block of material used in micromechanical analysis to find the effective properties of a composite material with the objective of replacing it with an equivalent homogeneous materials. In this sense, the RVE can be thought of as a bridge in a two-scale homogenization scheme. On the one hand, the RVE represents the domain of analysis in the microscale and on the other hand it is considered as a material point in the macroscale analysis. In other words, the composite will be defined in two scale: A microscopic scale defined by the RVE and a macroscopic scale defined by an equivalent homogenous material. This two-scale notion immediately motivates the need for average quantities.

4.2. Average theorem

Let V represents the volume of the RVE, then the volume average of a quantity Q over the RVE is

$$\bar{Q} = \frac{1}{V}\int_V Q\,dV \tag{7}$$

Eq. (7) provides the tool needed to state the average strain and stress theorems:

Average strain theorem: The average strain theorem can be stated as follows:

If a continuous body with perfect bonding between constituents is subjected to a homogenous boundary displacement $u_i^0 = \varepsilon_{ij}^0 x_j$ generated by a constant strain tensor ε_{ij}^0 along the boundary, then the average of the strain field inside the body is equal to ε_{ij}^0. This statement can be expressed as:

$$\bar{\varepsilon}_{ij} = \frac{1}{V}\int_V \varepsilon_{ij}\,dV = \varepsilon_{ij}^0 \tag{8}$$

Average stress theorem: The statement of the average stress theorem can be stated as follows:
If a heterogeneous body, in static equilibrium, is subjected only to a homogenous boundary traction $t_i^0 = \sigma_{ij}^0 n_j$ for which σ_{ij}^0 is a constant stress tensor along the boundary, then the average of the stress field inside the body is equal

to σ_{ij}^0. This statement can be expressed mathematically as

$$\bar{\sigma}_{ij} = \frac{1}{V}\int_V \sigma_{ij}\, dV = \sigma_{ij}^0 \tag{9}$$

where ε_{ij} and σ_{ij} are the pointwise strain and stress fields in the RVE. Depending on which of the average theorems is used, a homogenization problem could be either displacement driven in which case Eq. (8) is used or traction driven, in which case Eq. (9) is used. For the purpose of this work, the displacement driven approach will be utilised, hence all further development of the homogenisation scheme will be based on the displacement driven approach.

Hill's lemma and Hill-Mandel macrohomogeneity condition: Hill's lemma is given as

$$\left\langle \sigma_{ij}\varepsilon_{ij} \right\rangle - \bar{\sigma}_{ij}\bar{\varepsilon}_{ij} = \frac{1}{V}\int_V \left(\sigma_{ij}u_{i,j} - \bar{\sigma}_{ij}u_{i,j} - \sigma_{ij}\bar{\varepsilon}_{ij} + \bar{\sigma}_{ij}\bar{\varepsilon}_{ij} \right) dV \tag{10}$$

If the Hill-Mandel macrohomogeneity condition is satisfied, then the right-hand side of Eq. (10) vanishes so that

$$\left\langle \sigma_{ij}\varepsilon_{ij} \right\rangle = \bar{\sigma}_{ij}\bar{\varepsilon}_{ij} \tag{11}$$

Noting that equation $\left\langle \sigma_{ij}\varepsilon_{ij} \right\rangle$ is twice the value of the average strain energy U of the RVE, Eq. (11) allows us to write:

$$\bar{\sigma}_{ij} = \frac{\partial U}{\partial \bar{\varepsilon}_{ij}} \tag{12}$$

Let the constitutive relation of the equivalent homogeneous medium be

$$\bar{\sigma}_{ij} = D_{ijkl}^* \bar{\varepsilon}_{kl} \tag{13}$$

where D_{ijkl}^* represents the effective stiffness matrix. Considering Eq. (12) and Eq. (13), the effective stiffness matrix may be written as

$$D_{ijkl}^* = \frac{\partial \bar{\sigma}_{ij}}{\partial \bar{\varepsilon}_{kl}} = \frac{\partial^2 U}{\partial \bar{\varepsilon}_{ij}\partial \bar{\varepsilon}_{kl}} \tag{14}$$

4.3. Boundary condition

The boundary condition commonly applied in the analysis of an RVE is the homogeneous boundary conditions. This boundary condition when applied on the surface of a homogeneous body produces a homogeneous field. There are three types of homogeneous boundary conditions. These are homogeneous displacement, homogeneous traction and periodic boundary conditions. Let V be the volume of the RVE and ∂V be the boundary of V:
The Homogeneous Displacement Boundary Condition (HDBC) is obtained by imposing on the boundary surface displacement of the form:

$$u_i^0 = \varepsilon_{ij}^0 x_j \qquad \forall x_j \in \partial V \tag{15}$$

The Homogeneous Traction Boundary Condition (HTBC) is obtained by imposing on the boundary surface a traction

of the form:

$$t_i^0 = \sigma_{ij}^0 x_j \qquad \forall x_j \in \partial V \tag{16}$$

In the Periodic Boundary Condition (PBC), the displacement field u_i^0 over ∂V is of the form:

$$u_i^0 = \varepsilon_{ij}^0 x_j + \tilde{u}_i^0 \qquad \forall x_j \in \partial V \tag{17}$$

where $\tilde{u}_i^0$ is a displacement fluctuation that is assumed to be periodic over the RVE. That is, $\tilde{u}_i^0$ takes the same value at two homologous points on opposite face of the RVE.

5. Numerical results

In this section, a numerical example of homogenization problem will be solved to validate the PD homogenization scheme to be used. Thereafter, a numerical problem will be solved to study the effect of inclusion shape on the effective properties of composites.

5.1. Model validation

Before proceeding to achieve the objective of this work, a numerical problem will first be solved to validate the homogenization scheme. Consider a composite with long parallel cylindrical fibres as shown in Fig. 2a. The corresponding 2D RVE is depicted in Fig. 2b. The material parameters of the matrix and fibre are as follows: $E_{fiber} = 200\,\text{GPa}$, $\nu_{fiber} = 1/3$, $E_{matrix} = 100\,\text{GPa}$, $\nu_{matrix} = 1/3$. The problem is solved for fibre volume fraction $f = 0.6$. The RVE is subjected to a PBC.
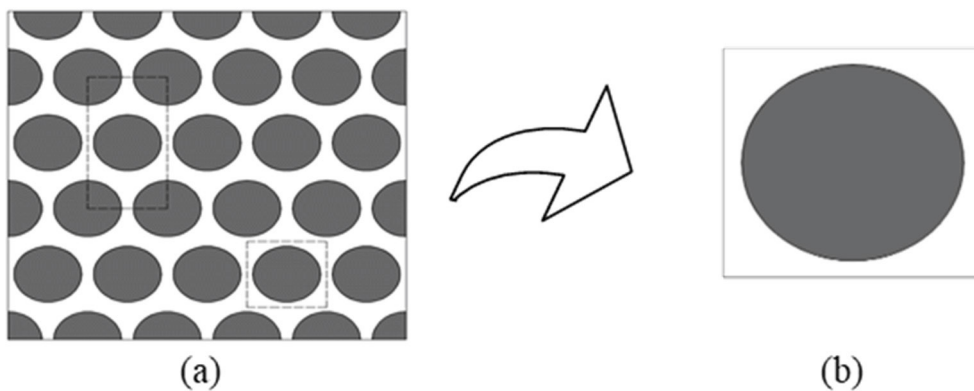

Fig.2. (a) Composite material, (b) RVE

This homogenization problem was solved using both Finite Element Method (FEM) and PD homogenization schemes. The deformed shape due to the application of loads on the RVE are shown in Fig. 3. The components of the effective stiffness tensor and hence the effective elastic modulus as obtained from the FEM and PD homogenization are shown in Table 1.
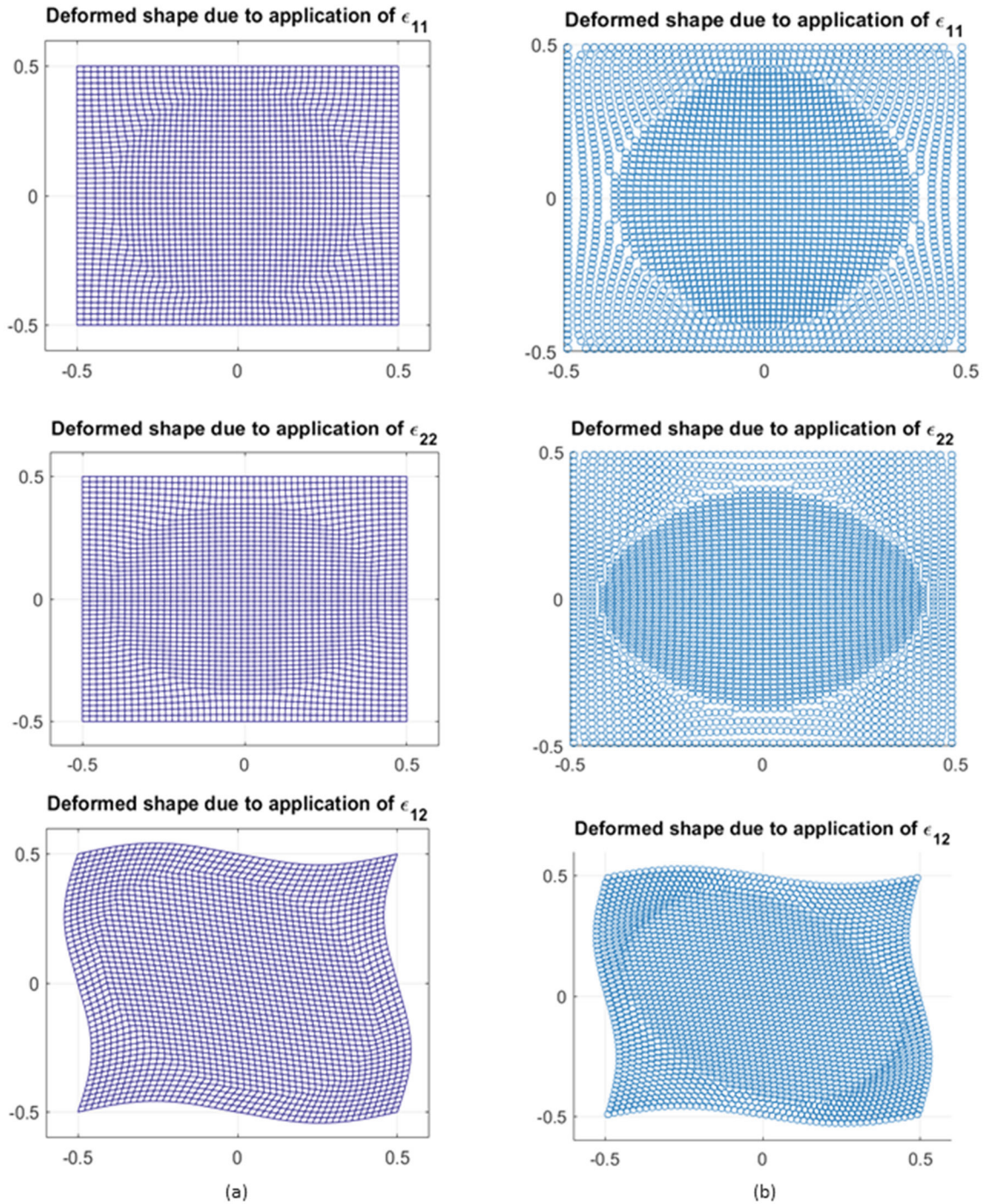
Fig. 3. Deformed shape of the RVE (a) FEM (b) PD

The effective elastic modulus obtained from both FEM and PD homogenization schemes from Table 1 shows that the PD homogenization scheme produces acceptable results.

Table 1. Result of homogenization using both FEM and PD for the purpose of model validation

Effective Quantity	FEM	PD
D_{1111}	1.6244×10^{11}	1.7062×10^{11}
D_{1122}	0.5257×10^{11}	0.6417×10^{11}
D_{1112}	0.000×10^{11}	0.0112×10^{11}
D_{2211}	0.5257×10^{11}	0.5808×10^{11}
D_{2222}	1.6244×10^{11}	1.7994×10^{11}
D_{2212}	0.000×10^{11}	0.5968×10^{11}
D_{1211}	0.000×10^{11}	0.0015×10^{11}
D_{1222}	0.000×10^{11}	0.0040×10^{11}
D_{1212}	0.4781×10^{11}	1.8117×10^{11}
Effective elastic modulus (E) Pa	1.4543×10^{11}	1.5084×10^{11}

5.2. Effect of inclusion shape

To study the effect of inclusion shape on the effective properties of composites, a composite with long parallel fibres of different shapes is considered. The material parameters of the matrix and fibre are as follows: $E_{fiber} = 200\,\text{GPa}$, $\nu_{fiber} = 1/3$, $E_{matrix} = 100\,\text{GPa}$, $\nu_{matrix} = 1/3$. The problem is solved for fibre volume fraction $f = 0.4$ and the RVE is subjected to a PBC.

The deformed shape of the RVE for different inclusion shape is shown in Fig. 4 and the effective modulus and Poisson's ratio for different inclusion shapes are presented in Table 2. A graph of perimeter of shape against the number of sides is shown in Fig. 5.

Table 2. Effective properties

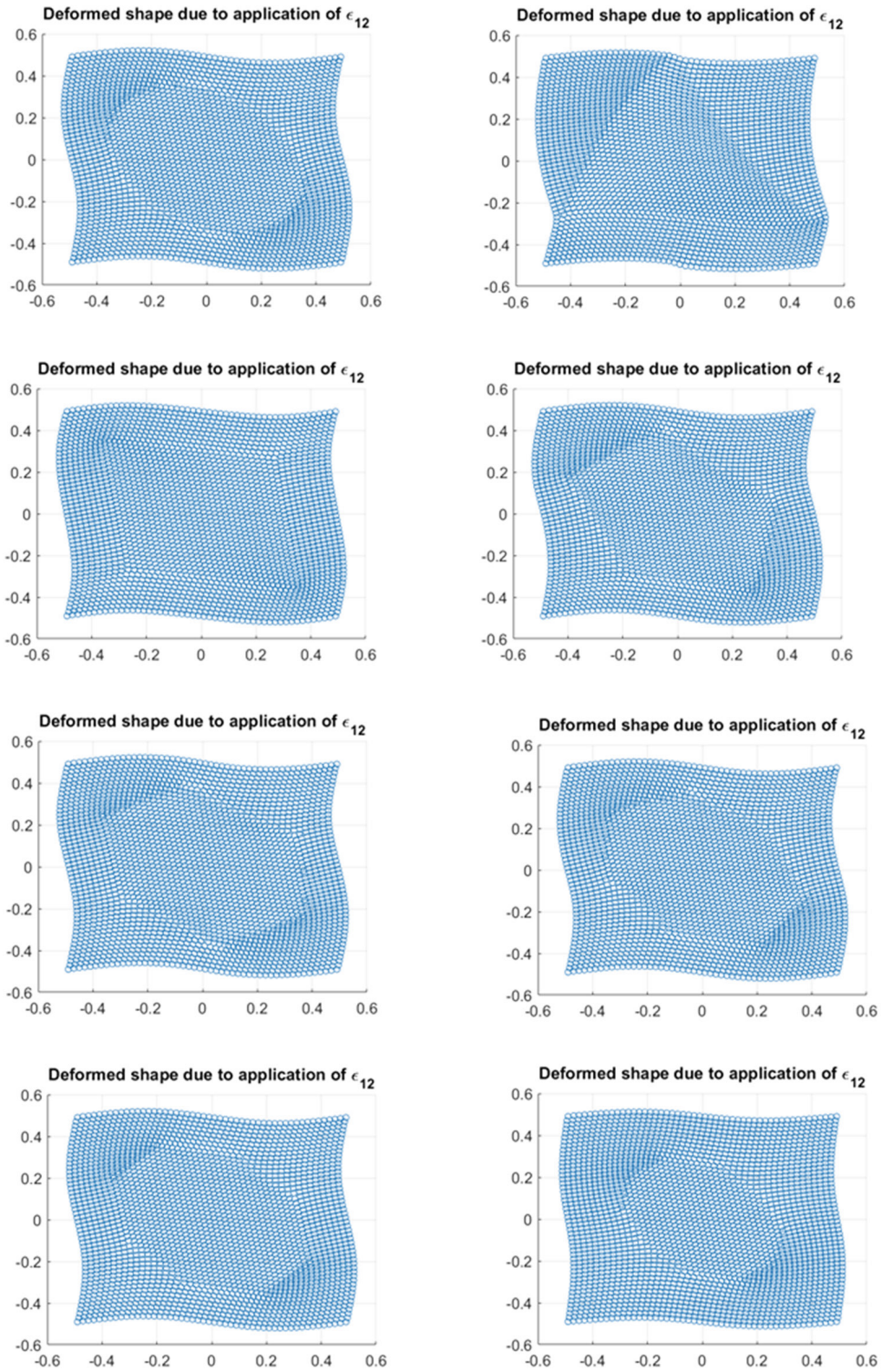| Shape	Area	No of Sides	Perimeter	Poisson Ratio	Effective modulus
Circle	0.4	1	2.242	0.34	1.33×10^{11}
Triangle	0.4	3	2.883	0.34	1.37×10^{11}
Square	0.4	4	2.530	0.34	1.34×10^{11}
Pentagon	0.4	5	2.411	0.34	1.35×10^{11}
Hexagon	0.4	6	2.354	0.34	1.35×10^{11}
Heptagon	0.4	7	2.322	0.34	1.33×10^{11}
Octagon	0.4	8	2.303	0.34	1.32×10^{11}
Decagon	0.4	9	2.280	0.34	1.24×10^{11}

Fig. 4. Deformed shapes of the RVE showing different inclusion shape
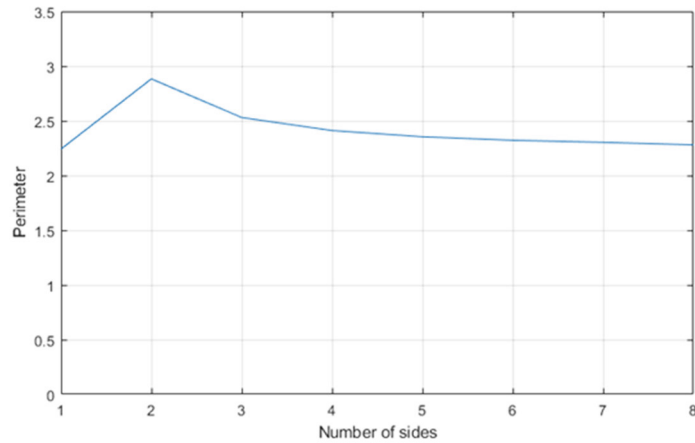
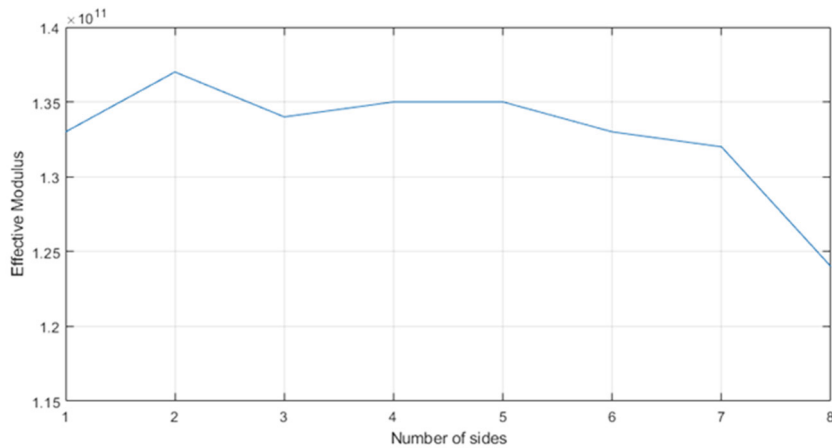Fig. 5. Perimeter of the different inclusion shapes

Fig. 6. Effective elastic modulus for different inclusion shapes

The graph shown in Fig. 6 shows an interesting trend. Generally, for a constant surface area of the inclusion, the elastic modulus shows a decreasing trend as the number of sides of the shape of inclusion increases. The highest value of the effective elastic modulus was recorded for triangular inclusion while the use of a decagon yielded the lowest effective elastic modulus.

6. Conclusions

In concluding, a bond-based PD homogenization scheme was developed to study the effect of inclusion shape on effective properties of composites. To validate the numerical scheme, results of homogenisation using this scheme were compared with those obtained using FEM. Results from both models show good agreement. Furthermore, analysis of the RVE using different inclusion shapes suggested a dependence of effective properties on shape of the inclusion.

Acknowledgements

References

Askari, E., Xu, J., Silling, S., 2006. Peridynamic Analysis of Damage and Failure in Composites. In 44th AIAA Aerospace Sciences Meeting and Exhibit, Reno, Nevada, USA, p. 88.

Baber, F., Ranatunga, V., Guven, I., 2018. Peridynamic modeling of low-velocity impact damage in laminated composites reinforced with z-pins. Journal of Composite Materials 52(25), 3491–3508.

Basoglu, M.F., Zerin, Z., Kefal, A., Oterkus, E., 2019. A computational model of peridynamic theory for deflecting behavior of crack propagation with micro-cracks. Computational Materials Science 162, 33–46.

Buryachenko, V. A., 2019. Computational homogenization in linear elasticity of peristatic periodic structure composites. Mathematics and Mechanics of Solids 24(8), 2497–2525.

Chen, X., Gunzburger, M., 2011. Continuous and discontinuous finite element methods for a peridynamics model of mechanics. Computer Methods in Applied Mechanics and Engineering 200(9), 1237–1250.

De Meo, D., Zhu, N., Oterkus, E., 2016. Peridynamic modeling of granular fracture in polycrystalline materials. Journal of Engineering Materials and Technology 138(4), 041008.

De Meo, D., Russo, L., Oterkus, E., 2017. Modeling of the onset, propagation, and interaction of multiple cracks generated from corrosion pits by using peridynamics. Journal of Engineering Materials and Technology 139(4), 041001.

Diyaroglu, C., Oterkus, E., Madenci, E., Rabczuk, T., Siddiq, A., 2016. Peridynamic modeling of composite laminates under explosive loading. Composite Structures 144, 14–23.

Diyaroglu, C., Madenci, E., Phan, N., 2019. Peridynamic homogenization of microstructures with orthotropic constituents in a finite element framework. Composite Structures 227, p. 111334.

Evangelatos, G.I., Spanos, P.D., 2011. A collocation approach for spatial discretization of stochastic peridynamic modeling of fracture. Journal of Mechanis of Materials and Structures, 6(7-8), 1171–1195.

Fallah, A.S., Giannakeas, I. N., Mella, R., Wenman, M. R., Safa, Y., Bahai, H., 2020. On the Computational Derivation of Bond-Based Peridynamic Stress Tensor. Journal of Peridynamics and Nonlocal Modeling.

Guo, J., Gao, W., Liu, Z., Yang, X., Li, F., 2019. Study of Dynamic Brittle Fracture of Composite Lamina Using a Bond-Based Peridynamic Lattice Model. Advances in Materials Science and Engineering 2019, p. 3748795.

Hill, R., 1963. Elastic properties of reinforced solids: Some theoretical principles. Journal of the Mechanics and Physics of Solids 11(5), 357–372.

Hu, W., Ha, Y. D., Bobaru, F., 2011. Modeling dynamic fracture and damage in a fiber-reinforced composite lamina with peridynamics. International Journal for Multiscale Computational Engineering 9(6), 707–726.

Hu, Y., Madenci, E., Phan, N.D., 2015. Peridynamic Modeling of Defects in Composites. In 56th AIAA/ASCE/AHS/ASC Structures, Structural Dynamics, and Materials Conference, Kissimmee, Florida, USA, p.1875.

Hu, Y.-l., Yu, Y., Wang, H., 2014. Peridynamic analytical method for progressive damage in notched composite laminates. Composite Structures 108, 801–810.

Imachi, M., Tanaka, S., Bui, T.Q., Oterkus, S., Oterkus, E., 2019. A computational approach based on ordinary state-based peridynamics with new transition bond for dynamic fracture analysis. Engineering Fracture Mechanics 206, 359–374.

Imachi, M., Tanaka, S., Ozdemir, M., Bui, T.Q., Oterkus, S., Oterkus, E., 2020. Dynamic crack arrest analysis by ordinary state-based peridynamics. International Journal of Fracture 221(2), pp.155–169.

Jiang, X.-W., Guo, S., Li, H., Wang, H., 2019. Peridynamic Modeling of Mode-I Delamination Growth in Double Cantilever Composite Beam Test: A Two-Dimensional Modeling Using Revised Energy-Based Failure Criteria. Applied Sciences 9(4), p. 656.

Kefal, A., Sohouli, A., Oterkus, E., Yildiz, M., Suleman, A., 2019. Topology optimization of cracked structures using peridynamics. Continuum Mechanics and Thermodynamics 31(6), 1645–1672.

Lehoucq, R.B., Silling, S. A., 2008. Force flux and the peridynamic stress tensor. Journal of the Mechanics and Physics of Solids 56(4), 1566–1577.

Liu, X., He, X., Wang, J., Sun, L., Oterkus, E., 2018. An ordinary state-based peridynamic model for the fracture of zigzag graphene sheets. Proceedings of the Royal Society A: Mathematical, Physical and Engineering Sciences 474(2217), p.20180019.

Madenci, E., Oterkus, E., 2014. Peridynamic theory. Springer, New York, NY.

Madenci, E., Barut, A., Phan, N. D., 2017. Peridynamic Unit Cell Homogenization. In 58th AIAA/ASCE/AHS/ASC Structures, Structural Dynamics, and Materials Conference, Grapevine, Texas, USA, p. 1138.

Madenci, E., Diyaroglu, C., Phan, N. D., 2018. ANSYS implementation of peridynamics for deformation of orthotropic materials, in 2018 AIAA/ASCE/AHS/ASC Structures, Structural Dynamics, and Materials Conference, Kissimmee, Florida, USA, p.1463.

Oterkus, E., 2010. Peridynamic Theory for Modeling Three-Dimensional Damage Growth in Metallic and Composite Structures. The University of Arizona.

Oterkus, E., Barut, A., Madenci, E., 2010a. Damage growth prediction from loaded composite fastener holes by using peridynamic theory. In 51st AIAA/ASME/ASCE/AHS/ASC Structures, Structural Dynamics, and Materials Conference 18th AIAA/ASME/AHS Adaptive Structures Conference, Orlando, Florida, USA, p. 3026.

Oterkus, E., Guven, I. and Madenci, E., 2010b. Fatigue failure model with peridynamic theory. In 12th IEEE Intersociety Conference on Thermal and Thermomechanical Phenomena in Electronic Systems, Las Vegas, Nevada, USA, p. 1-6.

Oterkus, E., Madenci, E., 2012a. Peridynamics for failure prediction in composites. In 53rd AIAA/ASME/ASCE/AHS/ASC Structures, Structural Dynamics and Materials Conference 20th AIAA/ASME/AHS Adaptive Structures Conference, Honolulu, Hawaii, USA, p. 1692.

Oterkus, E., Madenci, E., 2012b. Peridynamic theory for damage initiation and growth in composite laminate. Key Engineering Materials 488, 355–358.

Oterkus, E., Madenci, E., 2012c. Peridynamic analysis of fiber-reinforced composite materials. Journal of Mechanics of Materials and Structures 7(1), 45–84.

Oterkus, E., Guven, I., Madenci, E., 2012. Impact damage assessment by using peridynamic theory. Open Engineering 2(4), 523–531.

Oterkus, S., Madenci, E., Oterkus, E., Hwang, Y., Bae, J., Han, S., 2014, May. Hygro-thermo-mechanical analysis and failure prediction in electronic packages by using peridynamics. In 2014 IEEE 64th Electronic Components and Technology Conference (ECTC), Orlando, Florida, USA, p. 973-982.

Rädel, M., Willberg, C., Krause, D., 2019. Peridynamic analysis of fibre-matrix debond and matrix failure mechanisms in composites under transverse tensile load by an energy-based damage criterion. Composites Part B: Engineering 158, 18–27.

Ren, B., Wu, C. T., Seleson, P., Zeng, D., Lyu, D., 2018. A peridynamic failure analysis of fiber-reinforced composite laminates using finite element discontinuous Galerkin approximations. International Journal of Fracture 214(1), 49–68.

Rokkam, S.K., Truong, Q. T., Gunzburger, M., Goel, K., 2018. A Peridynamics-FEM Approach for Crack Path Prediction in Fiber-Reinforced Composites. In 2018 AIAA/ASCE/AHS/ASC Structures, Structural Dynamics, and Materials Conference, Kissimmee, Florida, USA, p. 0651.

Silling, S.A., 2000. Reformulation of elasticity theory for discontinuities and long-range forces. Journal of the Mechanics and Physics of Solids 48(1), 175–209.

Silling, S.A., Askari, E., 2005. A meshfree method based on the peridynamic model of solid mechanics. Computers & Structures 83(17), 1526–1535.

Seleson, P., Littlewood, D. J., 2016. Convergence studies in meshfree peridynamic simulations. Computers & Mathematics with Applications 71(11), 2432–2448.

Vazic, B., Wang, H., Diyaroglu, C., Oterkus, S., Oterkus, E., 2017. Dynamic propagation of a macrocrack interacting with parallel small cracks. AIMS Materials Science 4(1), pp.118–136.

Vazic, B., Oterkus, E., Oterkus, S., 2020. Peridynamic model for a Mindlin plate resting on a Winkler elastic foundation. Journal of Peridynamics and Nonlocal Modeling, pp.1–10.

Wang, H., Tian, H., 2012. A fast Galerkin method with efficient matrix assembly and storage for a peridynamic model. Journal of Computational Physics 231(23), 7730–7738.

Wang, H., Tian, H., 2014. A fast and faithful collocation method with efficient matrix assembly for a two-dimensional nonlocal diffusion model. Computer Methods in Applied Mechanics and Engineering 273, 19–36.

Wang, H., Oterkus, E., Oterkus, S., 2018. Predicting fracture evolution during lithiation process using peridynamics. Engineering Fracture Mechanics 192, 176–191.

Xia, W., Kasimu, Y. K., Oterkus, E., Oterkus, S., 2019. Representative volume element homogenization of a composite material by using bond-based peridynamics. Journal of Composites and Biodegradable Polymers 7, 51-56.

Weckner, O., Abeyaratne, R., 2005. The effect of long-range forces on the dynamics of a bar. Journal of the Mechanics and Physics of Solids, 53(3), 705–728.

Yang, Z., Oterkus, E., Nguyen, C.T., Oterkus, S., 2019. Implementation of peridynamic beam and plate formulations in finite element framework. Continuum Mechanics and Thermodynamics 31(1), 301–315.

Yu, W., 2016. An Introduction to Micromechanics. Applied Mechanics and Materials 828, 3–24.

Zhu, N., De Meo, D., Oterkus, E., 2016. Modelling of granular fracture in polycrystalline materials using ordinary state-based peridynamics. Materials 9(12), p.977.